

Deformation and adhesion of a periodic soft–soft nanocomposite designed with structured polymer colloid particles†

Fanny Deplace,^a Michael A. Rabjohns,^b Tetsuo Yamaguchi,^a Andrew B. Foster,^b Clara Carelli,^a Chun-Hong Lei,^c Keltoum Ouzineb,^d Joseph L. Keddie,^c Peter A. Lovell^b and Costantino Creton^{*a}

Received 2nd September 2008, Accepted 5th January 2009

First published as an Advance Article on the web 10th February 2009

DOI: 10.1039/b815292f

Although poor mechanical properties are usually found in films cast from waterborne colloidal polymers relative to their solvent cast counterparts, these materials offer the opportunity to control structure and composition very precisely at the nanoscale. Here, we introduce a knowledge-based strategy to design what we call a “soft–soft nanocomposite” in which a percolating crosslinked phase contains a second less crosslinked dispersed phase distributed regularly throughout it. This new type of structure uses polymer colloid particles as building blocks in a bottom-up approach to obtain simultaneously a very viscoelastic behaviour at small strains and an elastic behaviour at larger strains, bringing highly desirable properties for adhesives applications. For instance, the adhesion energy of the soft–soft nanocomposite on polyethylene is more than four times greater than that of a commercial material in which the particles are crosslinked and the interfaces are entangled. Our conclusions are broadly applicable to a large class of soft materials based on deformable polymeric networks, such as gels, elastomers and artificial tissues.

1. Introduction

Waterborne polymer colloids, commonly called latexes, provide a means to cast films for coatings, inks and adhesives that do not emit organic solvents into the atmosphere. Hence, these materials are able to meet increasingly tough legislation for reducing emissions of volatile organic compounds. A further attractive aspect of polymer colloids, that is far from being exploited fully, is that they provide a means to control film structure and morphology at the nanoscale. Each individual latex particle can be used as a building block. Nanostructure can be designed *into* each particle, such as in the commonly-used core–shell morphology.¹ Surface chemistry can be modified to provide a handle on the arrangement and packing of colloidal particles.² Furthermore, the particles can be used as a template for a regular nanoscale arrangement of nano-fillers³ or for other polymer phases.⁴ Finally, the enormous interfacial area between particles (equating to more than 10 m² g⁻¹ for particles of diameter 250 nm) offers a way to tailor bulk mechanical properties of films through the connectivity between particles.

Despite the environmental and legislative push, high-performance waterborne films for adhesives applications have not emerged mainly because of a lack of a clear identification of the

molecular architecture and microstructure needed to optimize the mechanical properties and of a lack of knowledge-based methods to achieve it. With the target structures having recently become clearer through careful experiments performed on solution and melt-processed adhesives,^{5,6} we developed and herein report, a method of colloidal processing to achieve precisely such structures, optimized for soft adhesives in the demanding application of adhesion to polyolefin surfaces.

Several studies have appeared on nanostructured films made from colloidal processing. They focus however either on core–shell particles^{1,7,8} with a hard–soft combination^{1,8} or on blends of colloidal particles with hard fillers.^{3,4,9–11} Studies on core–shell structures show that the shells of the particles can form a percolating structure which significantly affects the mechanical properties of the final material. If the shell is rubbery and the core is glassy, the film made from core–shell particles can be significantly softer than an equivalent blend of soft and hard particles,⁷ while if the shell is glassy than the matrix is rubbery, the opposite is true.¹ In the case of hard nanofillers, the colloidal processing is a way to obtain very homogeneously dispersed nanofillers³ although the pH of the latex can significantly affect the final structure.^{10,11} These fillers usually stiffen the material, which is of limited use for soft adhesives of interest here. Only one study has appeared discussing soft–soft nanocomposites with core–shell particles, but the contrast was not due to differences in cross-linking but by the presence of a significant amount of hydrophilic acrylic acid in the shell. Additional contrast was obtained with differential swelling with preferential solvents before mechanical testing.¹²

Our study specifically focuses on the effect of nanostructuring on the optimization of properties of soft adhesives and hence of the nonlinear viscoelastic behavior. Soft adhesives are a special class of soft matter that stick to nearly any surface upon simple

^aLaboratoire de Physico-Chimie des Polymères et Milieux Dispersés, UMR7615 ESPCI-CNRS-UPMC, 10 Rue Vauquelin, 75231 Paris Cédex 05. E-mail: costantino.creton@espci.fr

^bSchool of Materials, The University of Manchester, Grosvenor Street, Manchester, M1 7HS, United Kingdom

^cDepartment of Physics, University of Surrey, Guildford Surrey, GU2 7XH, United Kingdom

^dResearch and Technology, Cytec Surface Specialties, Anderlecht Street 33, 1620 Drogenbos, Belgium

† Electronic supplementary information (ESI) available: Viscoelastic / hardening parallel model. See DOI: 10.1039/b815292f

contact.¹³ They must have a low elastic modulus and be very dissipative in the viscous sense (the property of a liquid) to stick by simple contact, even to a rough surface, but must also be resistant to creep (the property of a solid), to avoid slow failure under load. Physically- or chemically-crosslinked polymers above their glass transition temperature (T_g) are the only known types of material that offer this combination of properties which result from having a loose but sufficiently connected network of chains. Achieving such a network is not easy with a material made from latex particles. Achieving film strength requires sufficient interdiffusion to “heal” the particle/particle interfaces, but sufficient crosslinking inside each particle is required for good creep resistance. As a result the “classic” adhesive made from latex particles consists of a percolating network of entangled interfaces encapsulating microgelled particle cores.^{14–16}

Although empirical design rules adapted to specific materials are prevalent in the patent literature, fundamentally-based general design principles for soft adhesives are virtually non-existent. The key reason for the lack of a design guideline is that adhesive debonding involves large-scale deformation of the adhesive itself, and only a careful control of the nonlinear large strain properties can lead to a knowledge-based design.¹⁷ Yet large strain properties of polymeric materials above their T_g are mainly controlled by their entanglements and crosslinking.^{18,19} In order to design high-performance soft adhesive materials it is therefore essential to control finely the interplay between entanglements and crosslinks.^{6,20,21}

One strategy which has recently proved to be successful in improving the adhesive properties of a soft rubber on a hard surface²² is to alternate soft elastic domains with soft viscous domains. A poorly-crosslinked material is very extensible and viscoelastic, whereas a densely-crosslinked polymer is much more elastic and less extensible. A strategy to achieve a structure with alternating elastic and viscous domains is to design a material with a spatially-varying crosslink structure. Emulsion polymerization produces latexes with particle sizes ranging typically between 100 and 400 nm, which represent the unit cell of the material. Controlling the structure of the particles and then the connectivity at the interfaces between particles provide two tools to design soft–soft nanocomposites. Both tools have been previously used to design coatings or adhesives from latexes,^{8,23,24} but the two have not been used in tandem to control nonlinear viscoelasticity, and well-defined structure-property relationships have not yet emerged.

2. Experimental

Synthesis

The model latexes were synthesized at 51.5 wt% solids using two-stage monomer-starved semi-batch emulsion polymerizations in which the particle core and shell are formed sequentially in a single preparation. The first stage, in which the particle core was formed, was taken to 96–97% monomer conversion before starting polymerization of the shell co-monomer mixture which was taken to >99.7% conversion. The co-monomer mixture used for the syntheses of both the core and the shell was designed to produce acrylic copolymers suitable for use as soft adhesives. The latexes comprised statistical copolymers of 66 wt%

2-ethylhexyl acrylate, 10 wt% *n*-butyl acrylate, 15 wt% ethyl acrylate, 0.4 wt% methacrylic acid (MAA), 2 wt% acrylic acid and 5 wt% styrene as the principal monomers. The shell comonomer composition was the same as for the core stage, except for the inclusion of diacetone acrylamide (DAAM) at a level such that its overall level in the whole particle was 0.4 wt% (Fig. 1). The level of chain transfer agent was at 0.1% in both core and shell for the adhesives in Fig. 3 and 0.15% in the core and 0.037% in the shell for the adhesive shown in Fig. 2. The DAAM-containing particles are able to crosslink and form a network by the reaction of the ketone carboxyl with a water soluble hydrazide during film formation and evaporation at room temperature as shown in Fig. 1.

The system in Fig. 3 was designed specifically to keep constant the total amount of DAAM whilst distributing it in shells of different thicknesses. The 0/100 latex was synthesized in a single step. The stoichiometric amount of adipic acid dihydrazide (ADH) for a complete reaction (Fig. 1) was calculated to give a 1 : 2 molar ratio of ADH : DAAM. In these calculations, it was assumed that all DAAM in the outer shell layer was available for reaction with ADH. The stoichiometric amount of ADH was added to the latex as a 2 wt% aqueous solution.

The classically crosslinked latex is a commercial latex made from homogeneous particles with a similar monomer composition to our model systems and was kindly provided by Cytec, Belgium.

Rheological and tensile tests

Dynamic mechanical properties were investigated using a newly-designed microrheometer.²⁵ It is based on a sphere-on-flat contact configuration designed to characterize the linear viscoelastic properties of thin films. Hence, identical films can be studied in both tack and rheology experiments.

Viscoelastic properties were measured by determining the lateral response of a macroscopic contact between a thin and confined adhesive layer and a rigid lens. Low amplitude (to avoid micro-slip), lateral sinusoidal motions were applied to the adhesive layer. The storage and loss moduli, over frequencies ranging between 0.1 and 10 Hz, have been calculated from the measured contact stiffness.²⁵

Tensile tests were performed on a standard tensile testing machine (JFC TC3) equipped with a non-contacting laser extensometer (Tinius Olsen H500L). Sample specimens were rectangular with an initial width of 4 mm and thickness of about 800 μm ; the initial length between the clamps was 17 mm. The constant crosshead velocity was chosen at 50 mm min^{-1} corresponding to initial strain rates of about 0.05 s^{-1} . All tests were carried out at room temperature and repeated five times for each condition.

Probe tack tests

The studies of adhesive performances have been made using the probe tack test. In this test a flat ended probe (of a diameter 10 mm) is brought into contact with a thin adhesive layer (with a thickness of $\sim 100 \mu\text{m}$) previously deposited and dried on a glass slide and is then removed at a fixed velocity.²⁶ A polished stainless steel probe and a probe coated with polished

polyethylene were used as standard probe surfaces. The surface roughness was well controlled to an average root mean square value of 0.1 μm . The same probe was used throughout a series of tests, and its flat end was cleaned after each measurement with water and acetone in the case of stainless steel and ethyl acetate in the case of polyethylene.

The probe tack tests have been carried out at room temperature on a custom-designed tester²⁷ with the following parameters: approach velocity = 30 $\mu\text{m s}^{-1}$; contact force = -70 N; contact time = 1 s; debonding velocity = 10 to 1000 $\mu\text{m s}^{-1}$. For each material five tests were performed. Although, for practical reasons all the stress-strain curves presented in this article correspond to a single experiment, they have been chosen to be representative of the five repeat tests that were carried out for each experimental condition. Values of adhesion energies are averages over these five tests. The fitting parameters of Table 1 and Table 2 were obtained from the fits of the tensile curves. Each experimental tensile curve (five per material) was fitted separately and Table 1 and 2 show the average values and standard deviation of the fit parameters.

Films were cast with a doctor blade on a glass slide and dried for about 12 h at room temperature and then 5 min at 110 $^{\circ}\text{C}$. The dry thickness was close to 100 μm . Characterizing the kinetics of the crosslinking reaction is of course important to make sure that the properties of the dry adhesive films are stable in time. Our results showed that the crosslinking reaction did not result in any further change of mechanical properties of the films after drying for 12 h at room temperature followed by 5 min at 110 $^{\circ}\text{C}$ in the oven.

AFM imaging

The structure in the bulk of the films was determined using atomic force microscopy (AFM) of cross-sections of the films. Images were obtained from a commercial instrument (NT-MDT Integra, Moscow, Russia) with intermittent contact. All scans used a silicon cantilever (ATEC-NC, Nanosensors, Switzerland) equipped with an ultrasharp, conical silicon tip having a radius of curvature less than 10 nm. The nominal resonant frequency of the cantilever was 330 kHz and its spring constant was about 45 N m^{-1} . This high cantilever stiffness plus a high tapping amplitude were required to overcome adhesion of the tip to the adhesive surface.²⁸

Films were cast on 50 μm thick poly(ethylene terephthalate) (PET) sheets and dried. Then a second PET sheet was laminated onto the adhesive surface. A cryogenically-cooled microtome (Nova Ultratome), equipped with a diamond knife with its edge normal to a freshly-cut edge of the laminate, was used to remove thin cross-sectional slices at a temperature of -120 $^{\circ}\text{C}$, at which the polymer was glassy. The laminate was mounted on the AFM stage such that its cross-sectional surface was facing upwards and horizontally. AFM was performed on this sliced surface.

3. Nanocomposite design and mechanical properties

As shown schematically in Fig. 1, we have used a three-stage process to synthesize the soft-soft nanocomposite in a bottom-up approach. In the first stage, we employed emulsion polymerization to synthesize acrylic copolymer core particles which

provide the desired T_g (-38 $^{\circ}\text{C}$) and level of viscoelasticity. Then in the second emulsion polymerization stage, the particles were grown to a diameter of ~ 250 nm with a comonomer composition that was altered slightly to incorporate a small amount of DAAM into the particle shell phase. The pendant reactive DAAM ketone groups in the copolymer are able to form crosslinks by reaction with amine groups from a component that is added to the aqueous phase. Thus, in the third stage, ADH was added to the aqueous phase to react with the shell-phase DAAM groups during drying of the latex film. The latex is deposited on a substrate with a doctor blade, and the water is left to evaporate. The close-packed particles deform into rhomboid dodecahedra to fill the available space (appearing like a honeycomb in two dimensions). Because the polymer has a very low T_g , interdiffusion occurs readily when the particles come into contact at room temperature.^{15,16} The ADH crosslinker reacts with the DAAM ketone groups slowly, thereby allowing interparticle interdiffusion to proceed initially, but eventually the crosslinking blocks any further diffusion, effectively freezing in place the original core-shell structure of the particles (Fig. 2). The DAAM-ADH crosslinking system was selected in preference to the many other crosslinking chemistries^{29,30} because it promotes interfacial crosslinking between particles and proceeds with an increasing rate as water is lost from the film,^{31,32} two factors that are key to the design principles introduced in this paper.

From the point of view of the macroscopic properties of the dry film, a key factor is that the crosslinking occurs within but also between particles, creating in effect a fully-percolating "honeycomb" structure of more crosslinked and elastic domains. Contained within this honeycomb are viscoelastic domains of the size of each particle core. AFM with intermittent contact provides evidence for the creation of a crosslinked honeycomb structure throughout the bulk of the 100 μm thick film. The AFM phase image of a cross-section of a core-shell latex film without any addition of the crosslinker is more homogeneous in comparison to a film with added crosslinker (Fig. 2a). The images present the phase lag, ϕ , of the photodiode output signal

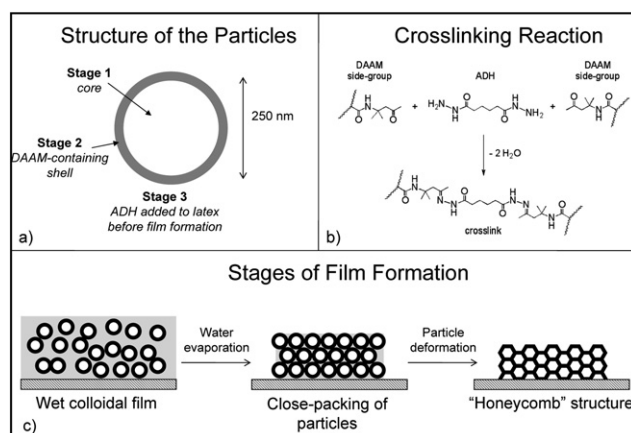


Fig. 1 Illustration of the synthesis, crosslinking chemistry and film formation process of the soft-soft nanocomposite films. (a) Particles are created in a two-stage process (core followed by the shell). (b) The particle shells are then interfacially crosslinked by reaction of DAAM with ADH (c) during the film formation process.

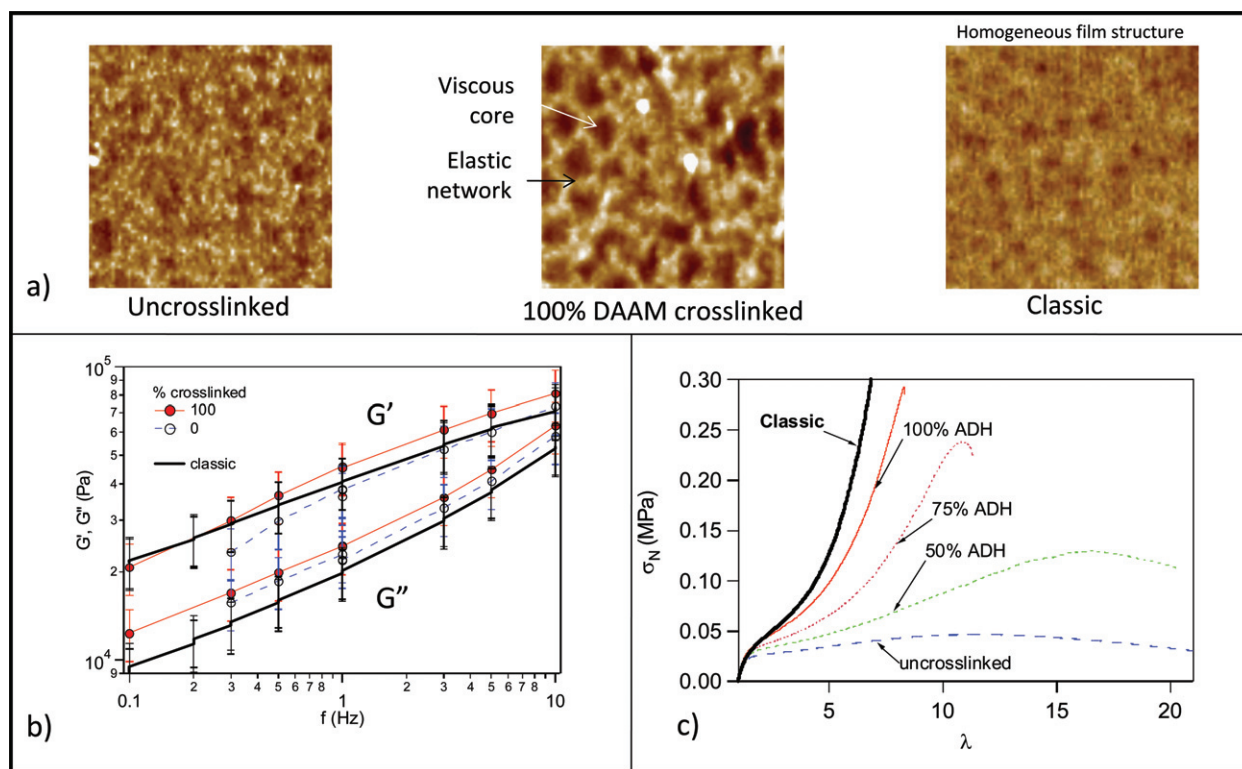


Fig. 2 (a) AFM phase images of the cross-sections of a 80/20 film without ADH crosslinker and with 100% ADH compared to the classically crosslinked latex. Darker regions in the images correspond to higher values of ϕ and therefore represent more energy dissipative regions, e.g. the particle cores. All image sizes are $1.5 \mu\text{m} \times 1.5 \mu\text{m}$. (b) Linear viscoelastic properties G' and G'' of the films measured as a function of the ADH/DAAM stoichiometric ratio. (c) Large-strain tensile tests of the same materials as a function of the ADH/DAAM stoichiometric ratio.

in relation to the driving piezoelectric signal as a function of position within the scan area. Changes in ϕ reflect variations in the energy dissipation, E_D , of the cantilever as its tip moves across a surface.³³ When the tip interacts with a viscoelastic region with a high viscous component, more energy will be dissipated, and therefore ϕ will be greater in comparison to a more elastic region.³⁴ The image indicates that an elastic percolating network is created upon the addition of the crosslinker.

The changes in the molecular structures are also evident from the mechanical properties. If we add various stoichiometric amounts of ADH to the same core-shell latex, the linear viscoelastic properties of the dry film do not change much, as shown in Fig. 2b. On the other hand, the large strain properties measured in a tensile test vary dramatically (Fig. 2c). In other words, the stiffness of the material at small strain is barely affected by the interfacial crosslinking, while the large-strain behaviour evolves from macroscopic flow (at 0% of crosslinking) to elastic, solid-like deformation (at 100% of crosslinking). This controlled variation of the large-strain properties of the nanocomposite without a marked change of the linear properties is impossible to obtain by a simple variation of the crosslinking within each particle by using a chain transfer agent and/or crosslinking agent during the polymerization. This additional tuneability offers distinct advantages in applications, as will be discussed later. For comparison, Fig. 2 also shows the morphology and properties of a commercial waterborne adhesive made from homogeneous

particles with approximately the same composition as the core polymer in the core-shell but with a “classic” uniform crosslinking inside each particle and none between particles. Fig. 2b shows that the loss modulus G'' of the interfacially crosslinked system can be maintained higher despite the addition of a crosslinking chemistry that brings the film to the level of cohesive values of the commercial sample (Fig. 2c).

Within this design scheme it is straightforward to vary systematically the levels of crosslinking within the shell and core by varying the amounts of chain transfer agent, DAAM and ADH and altering the relative volume fractions of the two phases. More extensive data will be presented in a forthcoming paper.³⁵ As an example of the design principle, three types of particles with strictly identical copolymer compositions and chain transfer agent content for the shell and the core, except for the DAAM content, were examined. The total amount of DAAM was kept constant at 0.4 wt% of total monomer but its spatial distribution varied from being homogeneous throughout the particle to being very localized on the outside of the particle, as shown in Fig. 3a. The three materials will be referred to as 0/100, 45/55 and 80/20, referring to the relative proportion (by volume) of the core and the DAAM-containing shell. All materials were crosslinked using 100% of the stoichiometric amount of ADH, thus introducing a density of crosslinks corresponding theoretically to $1.2 \text{ mol}\cdot\text{cm}^{-3}$. However, in the 0/100 material these crosslinks are homogeneously distributed throughout the particle, while for the 45/55 and 80/20, they are

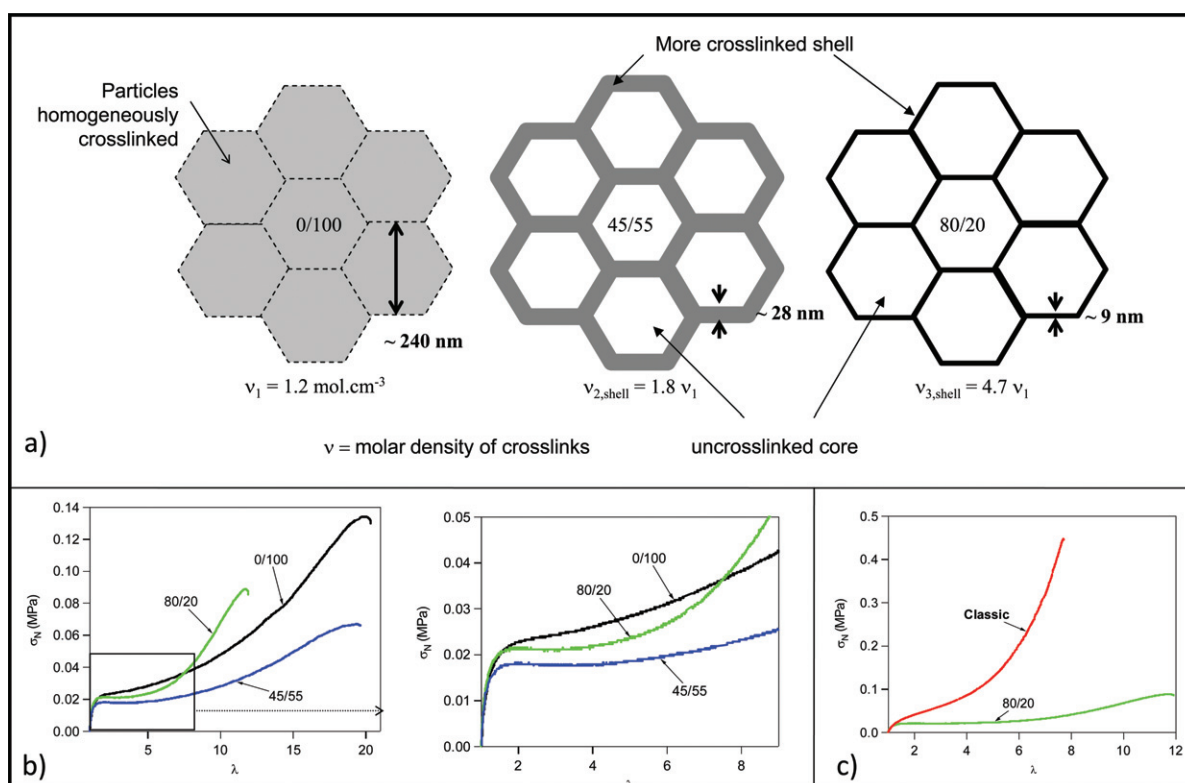


Fig. 3 (a) Schematic of the particles with different shell volumes of heterogeneous crosslinking and the corresponding crosslink densities. (b) Large-strain tensile tests showing the effect of the heterogeneity in the softening (a decreasing $d\sigma/d\lambda$ slope) and hardening (an increasing $d\sigma/d\lambda$ slope) behaviour of the same materials. (c) Large-strain tensile tests of the 80/20 compared to a classically crosslinked adhesive.

more localized on the outside of the particles and are of course denser. Fig. 3b shows that the initial modulus is not much affected by the change in the localization of the crosslinking points in the network. On the other hand, the nonlinear properties are changed significantly by this localization. The pronounced strain hardening observed at very large strains for all materials shows that the network is percolating. There is a more pronounced softening and earlier hardening evident for the material with a higher contrast between the elastic and viscous domains.

As a comparison we show in Fig. 3c the tensile properties of the nanostructured film alongside those of the “classic” film with a homogeneous structure (shown in Fig. 2a). To obtain the same modulus as the nanostructured film, a much higher level of crosslinking had to be used inside the particle while the particle interfaces are merely entangled. This structure led to much less strain softening at intermediate strains and a much more pronounced and early strain hardening.

4. Adhesive properties

These differences in large-strain behaviour without modification of the small-strain viscoelasticity have important consequences for the films’ adhesive properties.

The adhesive properties were determined accurately with a mechanical ‘probe’ test, which involves the controlled contact and removal of a cylindrical flat-ended probe from the adhesive film.^{26,27} Experimental details are provided; Fig. 4 shows a typical nominal stress versus nominal strain curve along with the

corresponding images captured simultaneously through the transparent substrate during the debonding process. The mechanism of failure invariably starts with the nucleation of cavities, and it is the growth of these cavities in the direction parallel or normal to the interface that determines whether the material is adhesive or not. The more the material can be extended before detaching from the surface, the higher is the adhesion energy W_{adh} , which is defined as the integral under the stress–strain curve multiplied by the initial film thickness.¹³

If we now compare the stress–strain curves for the interfacially-crosslinked materials with that of the classically crosslinked commercial material, the relevance of the pronounced softening becomes obvious. Average values of W_{adh} for the nanocomposite adhesives are significantly higher than those for the commercial benchmark adhesive on both steel and polyethylene surfaces and well in the range of permanent pressure-sensitive adhesives.

The details of the stress–strain curves reveal that, in all cases, the detachment of the adhesive proceeds with the formation of fibrils. However, the differences in adhesion energy do not arise from the level of stress necessary to stretch the fibrils (which is similar for the four materials) but rather from the maximum extension that can be applied to the fibril before detachment. Given the fact that the copolymer composition and the small-strain modulus are nearly identical for all materials, the differences are not due to interfacial interactions but rather to the differences in large-strain properties. The comparison between Fig. 5a and 5c shows the coupled effect of strain

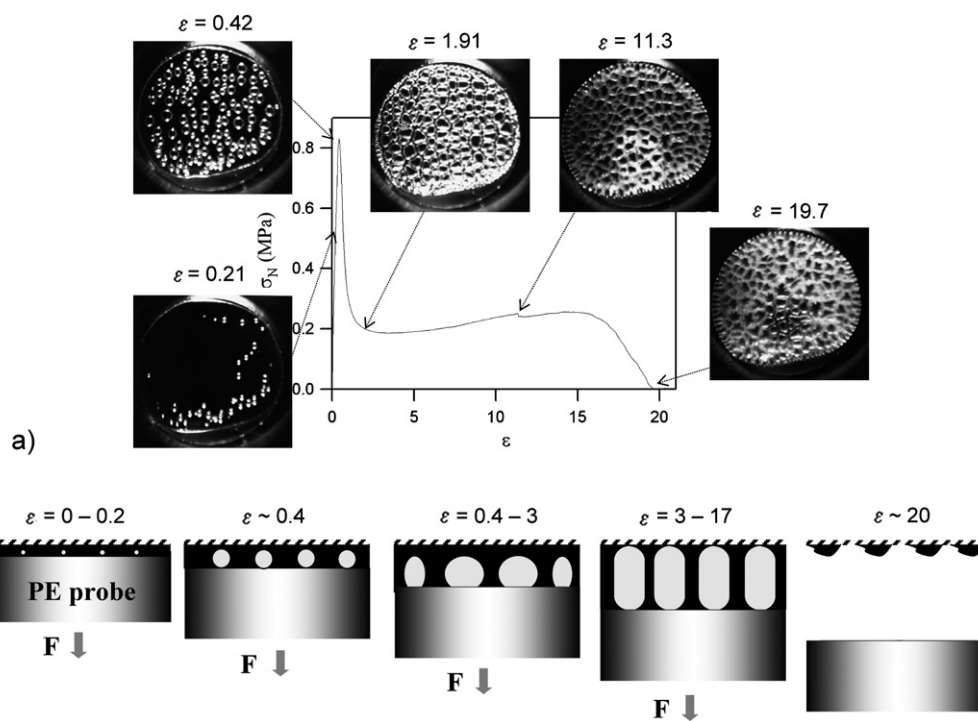


Fig. 4 (a) A typical probe test stress–strain curve with the corresponding images showing the appearance of cavities under tensile stress and their growth in the plane of the substrate. (b) The lower images show a schematic side view of the growth of the cavities.

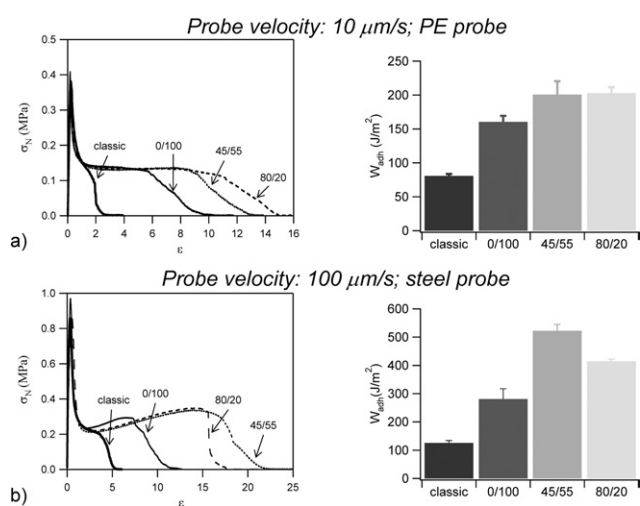


Fig. 5 (a) Stress–strain curves obtained in probe tests and values of the adhesion energy for these four adhesives when debonded from a polyethylene (PE) surface at a velocity of $10 \mu\text{m s}^{-1}$. (b) Stress–strain curves obtained in probe tests and values of the adhesion energy for these four adhesives when debonded from a steel surface at a velocity of $100 \mu\text{m s}^{-1}$.

hardening and viscoelastic relaxation.³⁶ In effect, the pronounced strain softening observed for the 80/20 soft–soft nanocomposite in tensile experiments allows a large deformation of the fibril before detachment. This effect is only observed for the adhesion on polyethylene surfaces where resistance to interfacial crack propagation are important.³⁷ On steel surfaces, the viscoelastic behaviour is less important, and it is the onset of strain hardening (occurring later for the 45/55 material) which

dominates the behaviour. Although the effect is clear, the difference in behaviour between the steel and the polyethylene surface are magnified by the choices of probe velocities. In general low probe velocities emphasize differences in viscoelastic dissipation while high velocities tend to be surface-insensitive and reflect more the differences in the onset of strain hardening at very high strains.

In all cases, the interfacial crosslinking and pronounced softening followed by an eventual strain hardening produces a much more stable fibril structure for the same initial modulus.

In more general terms, viscoelastic strain softening is known to have important consequences for the fracture behaviour of materials.³⁸ It favours crack blunting and hence slows down or stops crack propagation. This is a highly desirable property of liquids but is more difficult to achieve in solids. Strain softening is usually due to the breakdown of an organized structure and has been reported for several nanocomposites,^{1,39,40} the most widespread of which are simply the carbon-black filled rubber.⁴¹ However, our soft–soft nanocomposite represents the first example where enhanced strain softening has been obtained on purpose from a polymer network without fillers but instead through a specific design of the heterogeneity of the crosslinking.

5. A simple model

Since these differences in large-strain behaviour are essential for the adhesive and fracture properties, it is worthwhile and illustrative to model them with a simple mechanical model combining the properties of a viscoelastic fluid (representing the core) and a strain-hardening elastic solid (for the shell). The simplest example of such a model described briefly here, see ESI† for

details, is the parallel combination of the Upper Convected Maxwell (UCM) model, classically used in fluid mechanics to describe the flow of viscoelastic fluids,⁴² with the Gent strain-hardening model,⁴³ recently proposed to describe the fully-elastic deformation of rubbery networks and including the finite extensibility of polymer chains in the network. Admittedly using the convected derivative is not necessary to fit uniaxial tension data, but our long-term goal was here to eventually use such a model for numerical simulations of more complex geometries.

A prediction of the uniaxial stress–strain curve can be extracted from the constitutive model and comes out as the sum of contributions to the stress from the UCM element and the Gent element, which can be written as:

$$\sigma_N(\lambda) = \sigma_{N,v}(\lambda) + \sigma_{N,e}(\lambda) \quad (1)$$

where

$$\sigma_{N,v}(\lambda) = \left(\frac{2G_v D_e}{1 - 2D_e} \left(1 - \exp\left(-\frac{(1 - 2D_e)}{D_e}(\lambda - 1) \right) \right) + \frac{G_v D_e}{1 + D_e} \left(1 - \exp\left(-\frac{(1 + D_e)}{D_e}(\lambda - 1) \right) \right) \right) \cdot \lambda^{-1} \quad (2)$$

and

$$\sigma_{N,e}(\lambda) = \left(\frac{G_e}{1 - \frac{\lambda^2 + 2/\lambda - 3}{J_m}} (\lambda^2 - 1/\lambda) \right) \cdot \lambda^{-1} \quad (3)$$

where G_v is the initial shear modulus of the viscoelastic part, D_e is the Deborah number (the product of the relaxation time of the viscous component and the strain rate), G_e is the small-strain shear modulus of the elastic part, J_m is the maximum allowable value of the first strain invariant and λ is the extension ratio. Such a model, described schematically in Fig. 6a, captures the physics of a bicontinuous network of a crosslinked elastic phase and an uncrosslinked viscoelastic phase. Although the individual elements of the model are not new, they have never before been used together to describe a material's nonlinear properties. A simulation of the two contributions for a typical soft adhesive is shown in Fig. 6b. It is shown that to reproduce the behaviour of

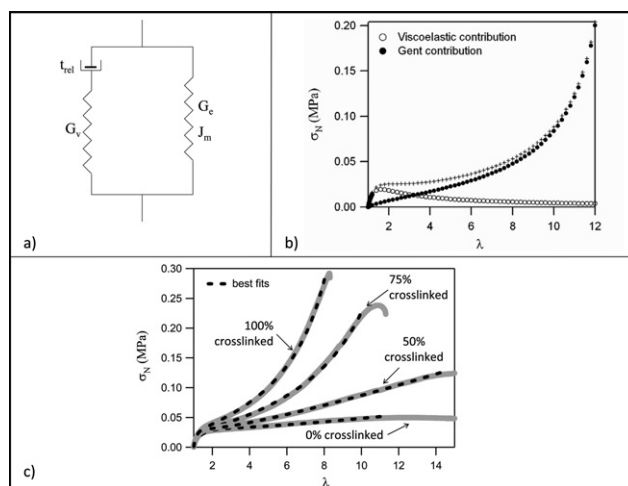


Fig. 6 (a) Schematic of the non-linear viscoelastic model used; (b) simulation of the non-linear viscoelastic and the elastic hardening contributions to the stress in a typical tensile test and (c) typical fits obtained on the curves presented in Fig. 2.

a good adhesive, a fast-relaxing viscoelastic contribution, which controls the initial modulus, coupled with a very soft elastic phase (invisible at small strains) with a finite extensibility is required. This is exactly what we achieved experimentally by separating spatially the viscoelastic and elastic contributions in the soft–soft nanocomposite.

The best fit of such a model with the tensile curves shown in Fig. 2 are presented in Fig. 6c. It is obvious that a very good fit can be obtained to the data; the values of the main parameters extracted from the fit are given in Table 1. The most obvious difference in behaviour between the materials is illustrated by the parameter J_m representing the finite extensibility of the network chains in the material. The sharp decrease in J_m as the amount of crosslinker is increased reflects the progressive formation of a tighter percolating structure of network chains. On the other hand, the values of G_v and G_e are influenced mainly by the initial structure of the polymer before interfacial crosslinking occurs. The sum of G_v and G_e corresponds to the high frequency unrelaxed shear modulus which is important during the early stages of debonding. As can be seen in Fig. 5, these early stages are not

Table 1 Fit parameters for the samples shown in Fig. 2

	G_v /kPa	G_e /kPa	J_m	D_e	G_v/G_e	$3(G_e + G_v)$ /kPa
no ADH	30.6 (± 2)	4.20 (± 0.4)	∞	0.382 (± 0.05)	7.30 (± 0.29)	104 (± 7.5)
50% ADH	47.4 (± 10)	7.76 (± 0.95)	3170 (± 750)	0.211 (± 0.07)	6.07 (± 0.58)	165 (± 32)
75% ADH	59.6 (± 7)	11.9 (± 1)	211 (± 21)	0.126 (± 0.03)	5.02 (± 0.32)	215 (± 24)
100% ADH	58.8 (± 4.01)	16.0 (± 0.5)	111 (± 4.6)	0.114 (± 0.02)	3.68 (± 0.20)	224 (± 13)
Classic	38.7 (± 6.89)	17.4 (± 6.89)	71 (± 6.89)	0.092 (± 0.013)	2.21 (± 0.23)	169 (± 25)

Table 2 Fit parameters for the samples shown in Fig. 3

	G_v /kPa	G_e /kPa	J_m	D_e	G_v/G_e	$3(G_e + G_v)$ /kPa
80/20	39.7 (± 3.10)	2.74 (± 0.212)	174 (± 12.7)	0.220 (± 0.021)	14.5 (± 0.418)	127 (± 9.91)
45/55	31.1 (± 1.84)	2.11 (± 0.080)	710 (± 153)	0.254 (± 0.006)	14.7 (± 0.467)	99.8 (± 5.72)
0/100	35.6 (± 3.32)	3.85 (± 0.105)	694 (± 131)	0.221 (± 0.048)	9.26 (± 1.12)	118 (± 9.65)

affected by the crosslinking, while the late stages and the large-strain behaviour are clearly affected by the interfacial crosslinking.

The effect of the localization of the crosslinking points in the shells of the original particles is shown in Table 2. The more pronounced softening of the more heterogeneous material, due to its more pronounced viscoelastic character at intermediate strains, is clearly visible in the ratio of G_v/G_e which increases with the degree of heterogeneity of the material. The relaxation time, and hence the Deborah number is used here as an adjustable parameter reflecting how fast the viscoelastic contribution to the modulus vanishes with time.

6. Conclusions

We have demonstrated how a soft–soft nanocomposite can be designed by film formation of latexes with structured particles and that the combined control of particle structure and interparticle crosslinking leads to very good spatial control of the polymer network structure, which in turn controls the nonlinear large-strain properties of the material. The interparticle crosslinking strategy facilitates use of a minimal amount of crosslinking when forming a percolating structure, while the particle structure allows the formation of a nanostructured material with domains of alternating higher and lower crosslink density. This last strategy maximizes the viscoelastic dissipation while retaining the percolating network structure which provides the strain hardening. The fracture of soft materials is highly influenced by crack blunting and by dissipation near the crack tip. We have demonstrated that introducing a viscoelastic dissipation mechanism, combined with a percolating network structure is essential to minimize creep, is a viable general strategy to increase the toughness of soft solids. While the target of this particular study was soft adhesives, these concepts of polymer network design are very general and applicable to all macromolecular soft materials, such as gels, rubbers, or artificial tissues.

Acknowledgements

We gratefully acknowledge funding from the FP6 project “Designed Nanoscale Heterogeneities for Controlling Water-Borne Pressure-Sensitive Adhesive Performance (NsHAPe)” (Contract No. NMP3-CT-2004-505442).

References

- 1 F. D. Dos Santos and L. Leibler, *J. Polym. Sci., Part B: Polym. Phys.*, 2003, **41**, 224–234.
- 2 E. C. Nelson and P. V. Braun, *Science*, 2007, **318**, 924–925.
- 3 T. Wang, C. H. Lei, A. B. Dalton, C. Creton, Y. Lin, K. A. S. Fernando, Y.-P. Sun, M. Manea, J. M. Asua and J. L. Keddie, *Adv. Mater.*, 2006, **18**, 2730–2734.
- 4 R. Mezzenga, J. Ruokolainen, G. H. Fredrickson, E. J. Kramer, D. Moses, A. J. Heeger and O. Ikkala, *Science*, 2003, **299**, 1872–1874.
- 5 C. Creton, in *Structure-Property Correlation and Characterization Techniques*, ed. K. Matyjaszewski, Y. Gnanou and L. Leibler, Wiley-VCH, Weinheim, Editon edn., 2007, vol. 3, pp. 1731–1752.

- 6 A. Lindner, B. Lestriez, M.S., R. Brummer, T. Maevis, B. Lühmann and C. Creton, *J. Adhes.*, 2006, **82**, 267–310.
- 7 Y. Chevalier, M. Hidalgo, J. Y. Cavaille and B. Cabane, *Macromolecules*, 1999, **32**, 7887–7896.
- 8 C. Schellenberg, K. Tauer and M. Antonietti, *Macromol. Symp.*, 2000, **151**, 465–471.
- 9 F. Dalmás, L. Chazeau, C. Gauthier, J. Y. Cavaille and R. Dendievel, *Polymer*, 2006, **47**, 2802–2812.
- 10 Y. Rharbi, B. Cabane, A. Vacher, M. Joanicot and F. Boue, *Europhys. Lett.*, 1999, **46**, 472–478.
- 11 J. Oberdisse, *Macromolecules*, 2002, **35**, 9441–9450.
- 12 Y. Rharbi, F. Boue, M. Joanicot and B. Cabane, *Macromolecules*, 1996, **29**, 4346–4359.
- 13 C. Creton, *MRS Bull.*, 2003, **28**, 434–439.
- 14 A. Zosel and G. Ley, *Macromolecules*, 1993, **26**, 2222–2227.
- 15 A. Aradian, E. Raphael and P. G. de Gennes, *Macromolecules*, 2002, **35**, 4036–4043.
- 16 M. A. Winnik, *Curr. Opin Colloid Interface Sci.*, 1997, **2**, 192–199.
- 17 L. Léger and C. Creton, *Phil. Trans., A*, 2008, **366**, 1425–1442.
- 18 M. Rubinstein and S. Panyukov, *Macromolecules*, 2002, **35**, 6670–6886.
- 19 P. G. de Gennes, *Scaling concepts in polymer physics*, 2nd edn., Cornell University Press, 1979.
- 20 A. Zosel, *J. Adhes.*, 1991, **34**, 201–209.
- 21 A. Zosel, *Colloid Polym. Sci.*, 1985, **263**, 541–553.
- 22 A. Majumder, A. Ghatak and A. Sharma, *Science*, 2007, **318**, 258–261.
- 23 V. L. Dimonie, E. S. Daniels, O. L. Shaffer and M. S. El-Aasser, in *Emulsion Polymerization and Emulsion Polymers*, ed. P. A. Lovell and M. S. El-Aasser, John Wiley, Chichester, Editon edn., 1997, pp. 293–326.
- 24 A. Aymonier, E. Papon, J.-J. Villenave, P. Tordjeman, R. Pirri and P. Gérard, *Chem. Mater.*, 2001, **13**, 2562–2566.
- 25 E. Gacoin, A. Chateauminois and C. Fretigny, *Polymer*, 2004, **45**, 3789–3796.
- 26 K. R. Shull and C. Creton, *J. Polym. Sci., B: Polym. Phys.*, 2004, **42**, 4023–4043.
- 27 H. Lakrout, P. Sergot and C. Creton, *J. Adhes.*, 1999, **69**, 307–359.
- 28 J. Mallégo, O. Dupont and J. L. Keddie, *Langmuir*, 2001, **17**, 7022–7031.
- 29 T. Y. Guo, J. C. Liu, M. D. Song and B. H. Zhang, *J. Appl. Polym. Sci.*, 2007, **104**, 3948–3953.
- 30 J. W. Taylor and M. A. Winnik, *J. Coat. Technol. Res.*, 2004, **1**, 163–190.
- 31 Y. Nakayama, *Prog. Org. Coat.*, 2004, **51**, 280–299.
- 32 H. P. Li, C. Y. Kan, Y. Du and D. S. Liu, *Polym. Adv. Technol.*, 2003, **14**, 212–215.
- 33 B. Anczykowski, B. Gotsmann, H. Fuchs, J. P. Cleveland and V. B. Elings, *Appl. Surf. Sci.*, 1999, **140**, 376–382.
- 34 W. W. Scott and B. Bhushan, *Ultramicroscopy*, 2003, **97**, 151–169.
- 35 F. Deplace, C. Carelli, A. Langenfeld, M. A. Rabjohns, A. B. Foster, P. A. Lovell and C. Creton, *J. Colloid Interface Sci.*, 2009, to be published.
- 36 N. J. Glassmaker, C. Y. Hui, T. Yamaguchi and C. Creton, *Eur. Phys. J., E*, 2008, **25**, 253–266.
- 37 C. Carelli, F. Deplace, L. Boissonnet and C. Creton, *J. Adhes.*, 2007, **83**, 491–505.
- 38 C. Y. Hui, A. Jagota, S. J. Bennisson and J. D. Londono, *Proc. R. Soc. London, Ser. A*, 2003, **403**, 1489–1516.
- 39 P. Podsiadlo, A. K. Kaushik, E. M. Arruda, A. M. Waas, B. S. Shim, J. D. Xu, H. Nandivada, B. G. Pumplun, J. Lahann, A. Ramamoorthy and N. A. Kotov, *Science*, 2007, **318**, 80–83.
- 40 H. Koerner, G. Price, N. A. Pearce, M. Alexander and R. A. Vaia, *Nat. Mater.*, 2004, **3**, 115–120.
- 41 E. H. Andrews, *Proc. Phys. Soc.*, 1961, **77**, 483–498.
- 42 R. B. Bird, R. C. Armstrong and O. Hassager, *Dynamics of Polymeric Liquids: Vol. 1 Fluid Mechanics*, 2nd edn., Wiley, New York, 1987.
- 43 A. N. Gent, *Rubber Chem. Tech.*, 1996, **69**, 59–61.